SETDB1 Restrains Endogenous Retrovirus Expression and Antitumor Immunity during Radiotherapy

Dong Pan[1], Xuhui Bao[1,2], Mengjie Hu[1], Meng Jiao[1], Fang Li[1], and Chuan-Yuan Li[1,3,4]

ABSTRACT

The type I interferon response plays a pivotal role in promoting antitumor immune activity in response to radiotherapy. The identification of approaches to boost the radiation-induced type I interferon response could help improve the efficacy of radiotherapy. Here we show that the histone methyltransferase SETDB1 is a potent suppressor of radiation-induced endogenous retrovirus expression. SETDB1 inhibition significantly enhanced the efficacy of radiotherapy by promoting radiation-induced viral mimicry to upregulate type I interferons. SETDB1 expression correlated with radiotherapy efficacy in human non–small cell carcinoma and melanoma patients. In a murine tumor model, genetic deletion of Setdb1 significantly enhanced radiotherapy efficacy, and Setdb1-deficient tumors had enhanced intratumoral lymphocyte infiltration, an observation confirmed in human cancer samples. Setdb1 deficiency led to increased basal and radiation-induced endogenous retrovirus (ERV) expression, enhanced MDA5/MAVS signaling, and upregulated type I interferons, which were essential for SETDB1 deficiency–induced radiosensitization. Taken together, these data suggest that inhibition of SETDB1 is a promising approach to enhance cancer radiotherapy efficacy by promoting radiation-induced viral mimicry and antitumor immunity through ERV induction.

Significance: The identification of the SETDB1-mediated suppression of radiotherapy-induced viral mimicry reveals SETDB1 inhibition as a potential approach to sensitize tumors to radiotherapy by enhancing the type I interferon response.

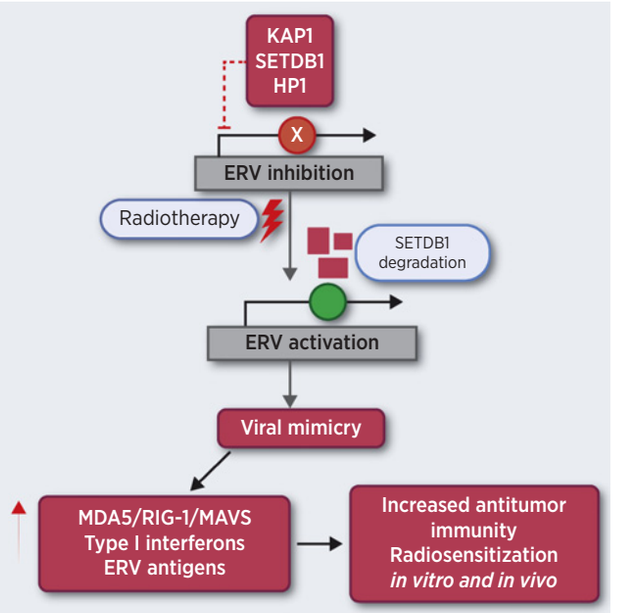

Loss of the histone methyltransferase SETDB1 leads to endogenous retrovirus (ERV) activation and increased antitumor immunity, boosting the effectiveness of radiotherapy.

Introduction

Radiotherapy is an established treatment modality involved in managing over 50% of all solid malignancies. Traditionally, radiobiologists believe that genomic DNA is the critical target of radiation damage in cancer cells, and the extent of radiation-induced DNA damage is the crucial determinant of tumor response to radiotherapy. Many research efforts had thus focused on enhancing radiotherapy by developing agents that could inhibit DNA double-strand break (DSB) repair. Recently, however, there has been an increasing recognition that additional molecular and cellular signaling pathways, especially those involved in regulating the immune system, may play significant roles in mediating tumor response to radiotherapy (1–4). For example, the cytoplasmic dsDNA-activated cGAS/STING pathway is a critical cellular defense mechanism against viral infections (5). In addition, a significant recent discovery in radiation biology is that cellular exposure to ionizing radiation can initiate cGAS/STING signaling, which activates the type I interferon response that plays a critical role in tumor response to radiotherapy (6–9). Consistently, a cytoplasmic endonuclease, Trex1, which can degrade cytoplasmic dsDNA, has a significant role in attenuating tumor response to radiotherapy because of its ability to downregulate cGAS/STING signaling (10).

Aside from cytoplasmic dsDNA-triggered cGAS/STING signaling, endogenous retroviruses (ERV) may be another significant factor in tumor response to radiotherapy. ERVs are vestiges of ancient retroviruses that account for 8% of the human genome (11). Most ERV sequences in the human genome are defective and cannot be activated. However, a small number of them are capable of being

[1]Department of Dermatology, Duke University Medical Center, Durham, North Carolina. [2]Department of Pathology, Duke University Medical Center, Durham, North Carolina. [3]Department of Pharmacology and Cancer Biology, Duke University Medical Center, Durham, North Carolina. [4]Duke Cancer Institute, Duke University Medical Center, Durham, North Carolina.

Corresponding Author: Chuan-Yuan Li, Dermatology, Duke University Medical Center, Box 3135, Durham, NC 27710. Phone: 919-613-8754; E-mail: chuan.li@duke.edu

Cancer Res 2022;82:2748–60

doi: 10.1158/0008-5472.CAN-21-3523

reactivated under the right circumstances. These can reinsert themselves into the genome and cause insertional mutagenesis (12). However, most of the activatable ERVs reside within the heterochromatin and are thus not active. Recently, several groups showed that DNA methyltransferase inhibitors such as 5-azacytidine can induce ERV activation, inducing a state of viral mimicry by generating cytoplasmic double-stranded RNAs (dsRNA). In addition, the ERV-derived dsRNAs can trigger the activation of the RIG-I–MDA5–MAVS signaling pathway, which stimulates the production of type I interferons and enhances immune-checkpoint blockade (ICB) therapy (13, 14). Researchers believe that 5-azacytidine treatment activated ERV transcription by desilencing of heterochromatin regions harboring the ERVs. Consistently, another group showed recently that inhibition of SETDB1, an essential histone methyltransferase that plays an integral role in maintaining the heterochromatin and suppressing ERV activation, can synergize with ICB therapy (15). In the present study, we decided to examine if SETDB1 plays any role in cancer radiotherapy. We discovered that radiation could induce a significant attenuation of SETDB1 expression, which caused a substantial downregulation of H3K9 trimethylation and activation of ERVs. Furthermore, SETDB1 deficiency could significantly boost ERV activation and accompanied type I interferon induction, sensitizing murine tumors to radiotherapy dependent on type I interferons and cytotoxic T cells. Therefore, we believe SETDB1 is potentially a promising target for enhancing cancer radiotherapy. An advantage of targeting SETDB1 is that it is a histone methyltransferase that is very amenable to drug development.

Materials and Methods

Cell culture and radiation exposure

We obtained A375 (human melanoma cell, ATCC; cat. #1619IG-2, RRID:CVCL_0132), A549 (human lung carcinoma cell, ATCC; cat. #CCL-185, RRID:CVCL_0023), HEK293T (ATCC; cat. #CRL-11268, RRID:CVCL_0063), CMT64 (mouse lung carcinoma cell, ECACC#10032301, RRID:CVCL_2406), and B16F10 (mouse melanoma cell, ATCC; cat. #CRL-6475, RRID_0159) from the Cell Culture Facilities of Duke University School of Medicine. A549 was grown in Ham's F-12K Medium (Sigma-Aldrich), A375, CMT64, and B16F10 were grown in high-glucose DMEM (Sigma-Aldrich), supplemented with 10% (v/v) FBS (Corning) and 1% penicillin/streptomycin (Thermo Fisher). Cells were cultured at 37°C in a humidified atmosphere containing 5% CO_2. All cell lines were subjected to a *Mycoplasma* test periodically using the Universal Mycoplasma Detection Kit (ATCC). In addition, we conducted X-ray irradiation using an XRAD 320 irradiator (Precision) with 320 kV and 12.5 mA at room temperature. The dose rate was 2.2 Gy/minute.

Drug treatment of irradiated cells

In some experiments, irradiated tumor cells were treated with tenofovir (100 μg/mL) and emtricitabine (60 μg/mL; Sigma-Aldrich), two anti-HIV drugs, to inhibit ERV activation. The dosage used was based on the effective doses previously reported (16). The drugs were administered to tumor cell culture 24 hours prior to irradiation.

In other experiments, MG132 (Sigma-Aldrich) was used to inhibit proteasome to determine if the proteasome was involved in the degradation of SETDB1. MG132 was dissolved in DMSO as 1 mmol/L stock solution. After the radiation, A549 cells were treated with 1 μmol/L MG132, and the cells were collected at different time points post-irradiation.

The Cancer Genome Atlas patient treatment and clinical data

We obtained patient treatment and clinical data from the cBioPortal database (https://www.cbioportal.org; ref. 17; RRID:SCR_014555), which includes 32 studies consisting of approximately 10,000 cancer patients and representing 33 types of cancer from The Cancer Genome Atlas (TCGA; ref. 18). Analyzed cohorts include non–small cell lung carcinoma (NSCLC; LUAD and LUSC) and SKCM TCGA PanCancer data within the time frame of our study (September 15, 2020–June 15, 2021).

Processing of TCGA RNA-seq and ERV data

TCGA patients' RNA-seqV2–scaled estimates were obtained from the cBioPortal database. In addition, we obtained ERV expression data for subsets of the TCGA cohort from a published study that quantified expression levels of transcribed ERVs by direct remapping from the raw RNA-seq data (19). In the SETDB1 and ERV correlation analyses ($n = 386$ for LUAD, $n = 123$ for SKCM), we only included patients for which both mRNA and ERV expression data were available

Gene set enrichment analysis

We carried out enrichment of genes ontology biological processes (BP) using the "ClusterProfiler" R software package (RRID:SCR_016884; ref. 20) with enrichment analysis performed for TCGA NSCLC and SKCM mRNA expression data sets. We deemed $P < 0.01$ as statistically significant.

CRISPR/Cas9-mediated gene knockout

We generated knockout cells by the use of lentivirus-mediated CRISPR/Cas9 technology. Supplementary Table S1 lists single-guide RNA (sgRNA) sequences targeting human and mouse genes. First, we cloned double-stranded oligos encoding the sgRNA sequences into BsmBI (Thermal Fisher Scientific) digested plasmid LentiCRISPRv2 (deposited by Dr. Feng Zhang of MIT to Addgene), which can coexpress Cas9 and sgRNA in the same vector. We then produced CRISPR lentivirus vectors in HEK293T cells by cotransfecting psPAX2 (RRID:Addgene_12660) and pMD2.G (RRID:Addgene_12259) plasmids with the sgRNA encoding plasmid according to the established protocol of the Zhang lab (21). Finally, we generated knockout cell lines by infecting target cells with lentivirus and cultured them in media with 1 μg/mL puromycin for A375, A549, and B16F10, 2 μg/mL for CMT64, and 1 mg/mL neomycin for A549 cells (which was transduced with a modified LentiCRISPRv2 vector with the neoresistant gene).

Cell proliferation assay

Cell proliferation was measured using an MTT Cell Proliferation Assay Kit (ATCC). Briefly, cells were seeded in a 96-well microplate at a density of 2×10^3 cells/well. About 10 μL MTT reagent was added to each well at different time points. After incubation at 37°C for 4 hours, adding 100 μL detergent reagent, we left the cells at room temperature in the dark for 2 hours. We then recorded the absorbance at 570 nm with a microplate reader. Each experiment was repeated three times.

Quantitative reverse-transcribed, real-time PCR

We carried out total RNA extraction using the RNeasy Mini Kit (Qiagen) following the manufacturer's protocol. We then conducted reverse transcription of the RNA with random hexamer primers using Superscript II reverse transcriptase (Invitrogen). We further performed qRT-PCR using the cDNA and 2× Quanti Test SYBR Green

PCR Master Mix Kit (Qiagen). We conducted all qRT-PCR under the following conditions: initiation for 10 minutes at 95°C, followed by 40 thermal cycles each at 95°C for 30 seconds and 60°C for 60 s. We calculated relative fold-change in mRNA expression calculated using the $2^{-\Delta\Delta C_t}$ method with the following equation: RQ (relative quantitation) $= 2^{-\Delta\Delta C_t}$. Supplementary Table S2 lists primers used for PCR of different genes.

Western blot

We first lysed cells in RIPA buffer with Protease Inhibitor Cocktail (Sigma-Aldrich). We then determined lysate total protein concentrations using the protein assay kit (Bio-Rad). Next, equal amounts of protein were denatured with sodium dodecyl sulfate (SDS) sample loading buffer (Bio-Rad) at 100°C for 10 minutes, then loaded onto a 10% SDS-PAGE gel for electrophoresis (SDS-PAGE). After electrophoresis, we transferred the proteins to a methanol-activated polyvinylidene fluoride membrane (Millipore) and blocked the membrane in tris-buffered saline [TBST; 10 mmol/L Tris-HCl (pH 8.0), 150 mmol/L NaCl, 0.1% Tween 20] containing 5% BSA (MP Biomedical) for 1 hour at room temperature and then incubated the membrane with primary antibodies overnight at 4°C. The primary antibodies include those against SETDB1 (Cell Signaling Technology; cat. #2196, RRID:AB_823637; and Proteintech; cat. #11231–1-AP, RRID:AB_2186069), GAPDH (1:1,000, Proteintech; cat. #60004–1-Ig, RRID:AB_2107436), MDA5 (Cell Signaling Technology; cat. #5321, RRID:AB_10694490), MAVS (Cell Signaling Technology, cat. #24930, RRID:AB_2798889; cat. #4983, RRID:AB_823566), IRF7 (Cell Signaling Technology; cat. #4920, RRID:AB_2127551), and $H3K9me^3$ (1:1,000, CST; cat. #13969, RRID:AB_2798355). After washing with TBST twice, the membrane was incubated with the appropriate horseradish peroxidase (HRP)-labeled secondary antibody for 1 hour at room temperature. Secondary antibodies conjugated with HRP included goat–anti-rabbit or mouse IgG (1:5,000). Finally, we visualized immunoblots using the enhanced chemiluminescence detection system according to the manufacturer's protocol.

Clonogenic survival assay after radiation exposure

To carry out the clonogenic survival assay, we first trypsinized the cells, washed the cells in PBS buffer, and exposed the cells to radiation in an Eppendorf tube. After radiation exposure, we seeded appropriate numbers of cells into 100-mm Petri dishes to produce colonies. For each radiation dose, we used three replicate dishes. Subsequently, we allowed the colonies to grow for 10 days, fixed the cells with 10 mL fresh Carnoy's solution (22), and stained them with 0.5% crystal violet for 20 minutes. Finally, we counted all colonies with more than 50 cells. We calculated the plating efficiencies (PE) as follows: the number of colonies formed/number of cells plated; survival ratios as follows: PE (irradiated)/PE (unirradiated).

Tumor growth delay studies

We purchased 6-week-old female C57BL/6J (RRID:IMSR_JAX:000664) and nude mice (RRID:IMSR:002019) from The Jackson Laboratory. Before tumor cell injection, we shaved the right hindlimbs of the mice. Next, we resuspended about 1×10^6 CMT64 or 1×10^5 B16F10 cells in 50 μL PBS and injected them into the shaved hindlimbs subcutaneously. After 7 days, we irradiated the tumors with 8 Gy of X-rays with the help of lead shielding. We then measured tumor volumes every other day and calculated tumor volumes using the following formula: (Length) × $(\text{Width})^2/2$. We sacrificed the mice when tumor volumes reached 2,000 mm^3. Finally, we used the Kaplan–Meier test and log-rank (Mantel–Cox) test for survival analysis among different tumor-bearing mice groups.

CIBERSORT analysis of the intratumoral lymphocyte infiltration in human tumors

CIBERSORT is a bioinformatics tool for characterizing the status of anticancer immunity and the proportion of tumor-infiltrating immune cells (23). We conducted a CIBERSORT analysis of NSCLC patients from the TCGA database based on their RNA expression data using an online CIBERTSORT analysis tool, TIP (http://biocc.hrbmu.edu.cn/TIP/), to visualize the immune cell subset of the tumor samples.

Quantifying tumor-infiltrating lymphocytes by flow cytometry

To quantify tumor-infiltrating lymphocytes, we established vector control and Setdb1KO B16F10 tumors established subcutaneously. First, we sacrificed tumor-bearing mice and excised the tumors on day 14 after inoculation. We then weighed and minced the tumors and incubated the tumor tissue in PBS solution with DNase I (50 μg/mL, Sigma) and collagenase P (2 mg/mL, Sigma) for 30 minutes at 37°C. Next, we passed the dissociated cells through a 70-μm cell strainer (BD). We then blocked the filtered cells with an anti-CD16/32 antibody (BioLegend; cat. #101319, RRID:AB_1574973) and stained them with specific surface antibodies (Pacific Blue anti-mouse-CD3 (BioLegend; cat. #100333, RRID:AB_2028473), APC anti-mouse CD4 (BioLegend; cat. #100424, RRID:AB_389324), APC-Cy7anti-mouse-CD8a (BioLegend; cat. #100766, RRID:AB_2572113), FITC anti-mouse CD45 (BioLegend; cat. #103107, RRID:AB_312972), BioLegend) for 20 minutes on ice. Next, we excluded the dead cells using Live/Dead Fixable Aqua dye (Thermo Fisher Scientific). Next, we fixed the cells with 2% PFA for 20 minutes and permeabilized them with 0.1% Triton X-100 PBS for 10 minutes on ice. After that, we incubated the cells with antibodies for intracellular targets (PE anti-mouse NK1.1, PE anti-mouse-Foxp3, APC IFNγ, and PE anti-mouse-GZMB, BioLegend) in the dark for 30 minutes on ice. We then analyzed the stained cells by use of a BD Canto flow cytometry system.

Immunofluorescence-based quantification of cytoplasmic dsRNA

We seeded the cells at 1×10^4 per dish into 35-mm glass-bottom poly-D-lysine–coated dishes (MatTek) before irradiating them. At various times after irradiation, we fixed the cells with 4% paraformaldehyde (PFA) for 20 minutes and permeabilized them with 0.5% Triton X-100 (Sigma-Aldrich) in PBS for 10 minutes. We then blocked nonspecific binding sites on the surface of the cells with 5% BSA in PBS for 60 minutes at room temperature before incubation with primary antibodies. We then incubated the cells with the primary antibody diluted in 5% BSA/1× PBS for 3 hours at room temperature. The primary antibody we used for immunostaining of dsRNA was J2 (1:200, SCICONS; cat. #10010200, RRID:AB_2651015), which specifically binds to dsRNA. After incubation, cells were washed three times with PBS, 10 minutes each, and then incubated with the appropriate Alexa Fluor 488/594 secondary antibodies (1:2,000, Invitrogen) diluted in 5% BSA for 1 hour. Next, we washed the cells three times with PBS for 10 minutes each time. We then counterstained the cellular nuclei with 4′,6-diamidino-2-phenylindole (DAPI, Thermo Fisher). Finally, we performed digital image analysis using a TCS SP5-inverted confocal microscope (Leica) at ×40 magnification. We used the ImageJ software (ImageJ, RRID:SCR_003070) to obtain the relative integrated fluorescence intensity per cell. We quantified images of 50 cells for every time point and carried out at least three independent experiments for each time point.

Lymphocyte depletion and interferon signaling blockade

We depleted $CD4^+$ T cells, $CD8^+$ T cells, and NK cells via i.p. injection of anti-CD4 (Bio X Cell; cat. #BE0003-1, RRID:AB_1107636), anti-CD8b (Bio X Cell; cat. #BE0223, RRID:AB_2687706), or anti-NK1.1 (Bio X Cell; cat. #BE0036, RRID:AB_1107737) at 100 μg per mouse, respectively, on days 1, 4, and 7 after tumor cell injection. We used an equal amount of IgG isotype antibodies (PIP, Bio X Cell) as a control. In addition, we injected an anti–IFNAR-1 antibody (Bio X Cell; cat. #BE0241, RRID:AB_2687723) i.p. at 200 μg per moue on days 6, 9, and 12 to block type I interferon signaling after tumor cell injection.

5-Ethynyl-2′-deoxyuridine incorporation assay and J2 costaining

We quantified cell proliferation fraction by the Click-iT EdU Cell Proliferation Kit (Thermo Fisher Scientific). Briefly, we seeded the cells at 1×10^4 per dish on 35-mm glass-bottom poly-D-lysine–coated dishes before radiation exposure. Four days later, we incubated the cells with 10 μmol/L 5-ethynyl-20-deoxyuridine (EdUrd) for 24 hours before fixing, permeabilizing, and staining the cells with EdUrd according to the manufacturer's protocol. We also carried out costaining of the cells with J2 antibody as described above.

Statistical analysis and reproducibility

We obtained TCGA patient treatment information, clinical data, and RNA sequence data from the cBioPortal database. We compared the difference in survival by using the log-rank (Mantel–Cox) test. We used the Spearman correlation test to conduct correlation analyses. In addition, we carried out gene set enrichment analysis and derived *P* values using the "ClusterProfiler" package in R software version 3.4.0. We used the unpaired *t* test to analyze the differences in CIBERSORT scores between different groups. We also used the unpaired *t* test to compare ERV expression levels between different groups.

For *in vitro* experiments, unless stated otherwise in figure legends, data are represented as individual values or as mean ± SEM. Group sizes (*n*) and applied statistical tests are indicated in figure legends. We assessed the statistical significance by using an unpaired *t* test analysis. Experiments were all performed at least three times with biologically independent samples.

For *in vivo* experiments, unless stated otherwise in figure legends, data are represented as individual values or as mean ± SEM. Group sizes (*n*) and applied statistical tests are indicated in figure legends. In all cases, we randomly assigned mice into different treatment groups stratified for tumor sizes at the time of treatment. In some experiments (as indicated in figure legends), we assessed the significance of the differences between different groups using the two-way ANOVA analysis. In other cases, we used the Mantel–Cox log-rank test to calculate the significance of the differences between different groups. Finally, we used GraphPad Prism 8.2.1 (GraphPad Prism, RRID: SCR_002798) for all of our statistical calculations.

Data availability statement

All of the data generated in this study are available within the article and the supplementary data files. In addition, we analyzed some data from the cBioPortal at https://www.cbioportal.org/study/summary?id=luad_tcga_pan_can_atlas_2018.

Results

Low SETDB1 expression predicts survival benefits in radiotherapy patients

To investigate whether SETDB1 expression levels influence human tumor response to radiotherapy, we analyzed the correlation between SETDB1 expression and response to radiotherapy in TCGA PanCancer lung and melanoma cohorts using the cBioPortal database (17). In particular, we analyzed subcohorts of 113 NSCLC and 45 melanoma (SKCM) patients known to have undergone radiotherapy (see Supplementary Table S3 and S4 for patient characteristics). Our analysis indicated that patients with low SETDB1 expression levels had a significant advantage in progression-free survival (PFS) when compared with those with high SETDB1 expression (high and low expressers divided by median; $P = 0.021$ or 0.030 for NSCLC or SKCM, respectively; **Fig. 1A** and **B**). Furthermore, although we used the median SETDB1 expression level to separate high versus low cohorts, Cox regression analysis using SETDB1 as a continuous variable shows that patient survival is negatively correlated with patient survival in both NSCLC and SKCM patients (Supplementary Fig. S1A and S1B). In NSCLC patients, the median of PFS was 41 months versus 17 months in SETDB1-low and -high groups, respectively. Among SKCM patients, the median PFS was 77 months versus 30 months in SETDB1-low and -high groups, respectively. Importantly, in the absence of radiotherapy, the differences in PFS between the SETDB1 high versus low groups became nonsignificant in NSCLC patients (**Fig. 1C**) and wholly gone in SKCM patients (**Fig. 1D**). Therefore, our analysis suggests that low SETDB1 expression may predict radiotherapy benefits in NCSLC and melanoma patients.

Based on the above analysis, we hypothesized that SETDB1 deficiency might sensitize tumors to radiotherapy. To evaluate the influence of SETDB1 on the intrinsic radiosensitivity of cancer cells, we generated SETDB1 knockout A549 human lung cancer and A375 human melanoma cells using the CRISPR/Cas9 technology (**Fig. 2A**; refs. 21, 24). We then carried out clonogenic surviving assays after exposing the cells to different doses of X-rays. Our results indicated SETDB1 deficiencies significantly decreased the clonogenic abilities of the A549 and A375 cells, especially at higher radiation doses (**Fig. 2B** and **C**). We also generated Setdb1KO B16F10 mouse melanoma cells and evaluated their radiation sensitivity. Our results indicate that similar to human tumor cells, Setdb1KO sensitized B16F10 cells at higher radiation doses (Supplementary Fig. S1C). Importantly, SETDB1 knockout has no effect on clonogenic (Supplementary Fig. S1D) and proliferative (Supplementary Fig. S1E) capacity of A549, A375, and B16F10 cells.

We next evaluated the influence of Setdb1KO on the radiotherapy response of murine CMT64 lung tumors (**Fig. 2D–F**) and B16F10 melanoma (**Fig. 2G–I**). After establishing subcutaneous tumors using vector control and Sefdb1KO CMT64 and B16F10 cells, we treated the tumors with radiotherapy. Our data indicated that Setdb1-deficient tumors grew slower than controls. Furthermore, they respond to radiotherapy significantly better than vector controls (**Fig. 2E** and **H**). Mice bearing Setdb1-deficient tumors also survived significantly longer (**Fig. 2F** and **I**), with tumors disappearing in 2 of 5 mice in both tumor models and not palpable at the end of the experiments.

Taken together, our experimental data suggest that SETDB1 deficiency sensitizes both murine tumors *in vivo* and human tumor cells to ionizing radiation *in vitro*, consistent with the observed radiotherapy benefits observed in SETDB1 cancer patients in TCGA NSCLC and SKCM cohorts.

SETDB1 deficiency promoted intratumoral lymphocyte infiltration

We next sought to elucidate the mechanisms of SETDB1 deficiency–induced sensitization of human and mouse tumors to radiotherapy. We started by conducting a gene ontology (GO) BP analysis (25, 26) of SETDB1 high- or low-expressing tumors in radiotherapy-treated

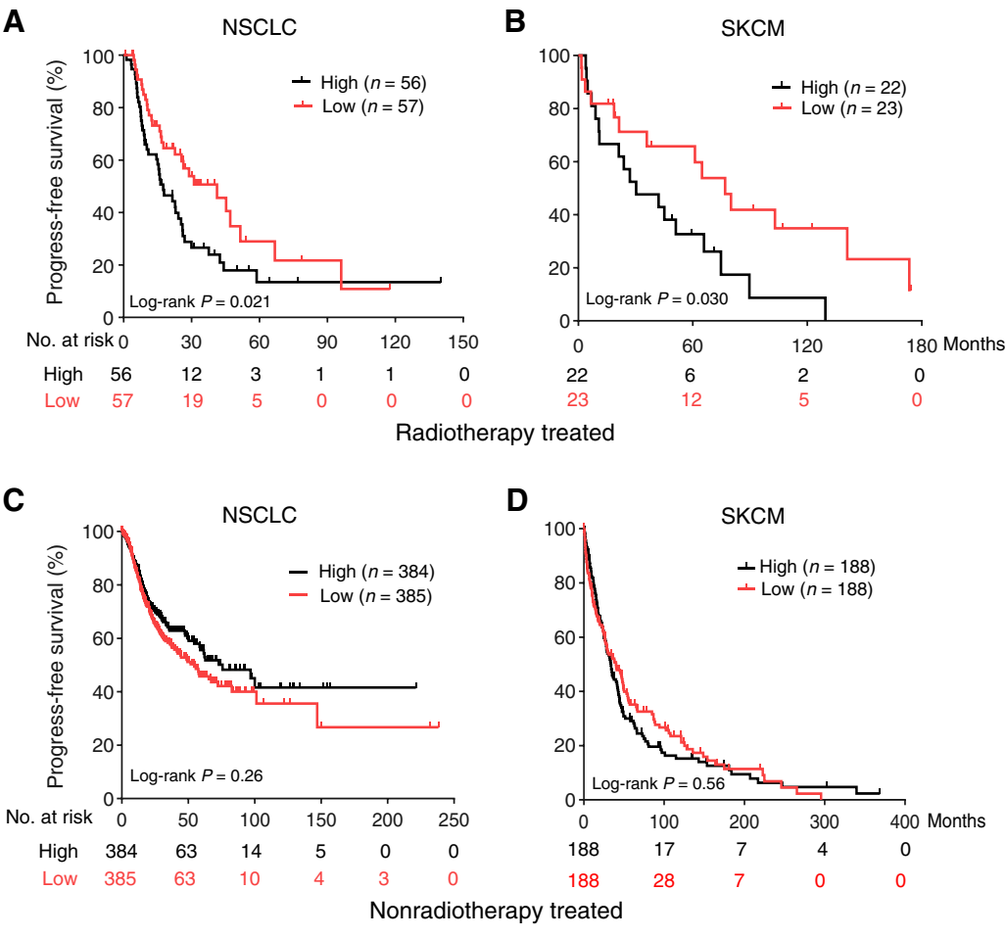

Figure 1.

The influence of the SETDB1 expression level on the PFS of radiotherapy patients. **A** and **B,** Kaplan–Meier analysis of the PFS of radiotherapy-treated TCGA NSCLC patients (**A**) and SKCM patients (**B**) with high or low SETDB1 expression. The cutoff value between high and low groups was the median. **C** and **D,** The PFS of nonradiotherapy treated NSCLC patients (**C**) and SKCM patients (**D**) with high and low SETDB1 expression. The cutoff value between high and low was the median. *P* values were determined by a log-rank test.

NSCLC and SKCM patients. There were 284 and 352 genes negatively correlated with SETDB1 expression in radiotherapy-treated NSCLC and SKCM patients. GO analysis showed that genes overexpressed in SETDB1 low-expressing NSCLC or SKCM tumors mainly belonged to innate immune response pathways such as leukocyte degranulation, myeloid cell activation, and neutrophil-mediated immunity. (**Fig. 3A** and **B**). In comparison, the numbers of genes overexpressed in the SETDB1 high expression group were 441 and 423 in NSCLC and SKCM patients, respectively. Furthermore, GO analysis indicated that the main pathways enriched in these tumors were related to RNA metabolism (**Fig. 3C** and **D**).

Based on the above GO enrichment analysis results, we reasoned that SETDB1-low tumors significantly activated genes involved in immune recognition and lymphocyte activation. To further examine this observation, we carried out CIBERSORT (27) analysis of SETDB1-high and -low, radiotherapy-treated TCGA NSCLC and SKCM patients using the TIP online database (28). CIBERSORT is a bioinformatics tool established to identify different immune effector subsets from RNA-seq data. Our CIBERSORT analysis showed that the recruitment scores for T, $CD4^+$ T cell, $CD8^+$ T, NK, DC, and macrophage cells were significantly higher in SETDB1 low versus high NSCLC patients (**Fig. 4A–F**). We made similar findings in SKCM patients except for $CD4^+$ T cells, which did not reach statistical significance despite a positive trend (**Fig. 4G–L**).

Based on our analysis that SETDB1-low expression correlated with increased intratumoral lymphocyte infiltration in TCGA NSCLC and SKCM patients, we assessed whether Setdb1 deficiency could boost intratumoral lymphocyte infiltration in murine tumors. For this purpose, we established Setdb1-deficient and control B16F10 tumors in syngeneic C57BL/6 mice and quantified the numbers of tumor-infiltrating lymphocytes using flow cytometry analysis following a gating strategy shown in Supplementary Fig. S2. Our analysis showed significantly increased $CD4^+$ and $CD8^+$ T-cell infiltration in Setdb1-deficient B16F10 tumors compared with control tumors (**Fig. 4M** and **N**). In addition, infiltrations of NK, $IFN\gamma^+CD8^+$ T cells in Setdb1-deficient B16F10 tumors also increased (**Fig. 4O** and **P**). Furthermore, there was a general trend toward increased infiltration of $CD4^+Foxp3^+$ Tregs and granzyme-B^+ ($GzmB^+$) $CD8^+$ cells. However, such increases did not reach statistical significance (**Fig. 4Q** and **R**).

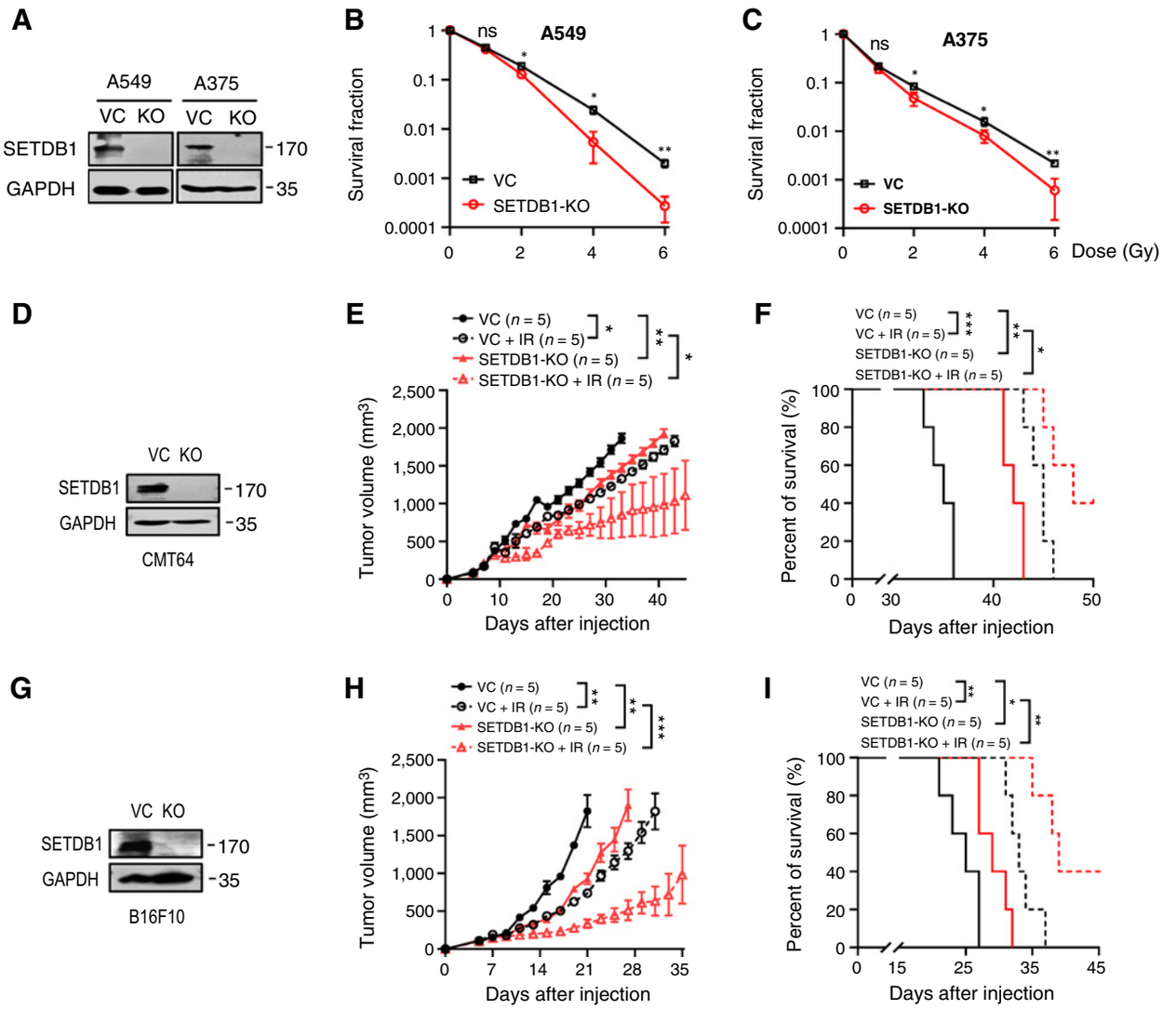

Figure 2.

The influence of SETDB1 knockout on radiosensitivities *in vitro* cells and tumors *in vivo*. **A,** Western blot analysis of SETDB1 expression in vector control (VC) and SETDB1 KO A549 and A375 cells. **B** and **C,** Clonogenic survival of VC and SETDB1 KO groups for A549 (**B**) and A375 (**C**) tumor cells exposed to different doses of X-rays. For both **B** and **C,** data were the aggregate of three independent experiments. **D,** Western blot analysis of Setdb1 levels in vector VC and Setdb1KO CMT64 cells. **E** and **F,** Tumor growth delay (**E**) and Kaplan–Meier survival curves (**F**) of C57BL/6 mice inoculated with 1×10^6 VC or Setdb1KO CMT64 cells. Radiotherapy (1×8 Gy) was conducted 7 days after inoculation of the tumor cells. **G,** Western blot analysis of Setdb1 levels in VC and Setdb1 KO B16F10 cells. **H** and **I,** Tumor growth delay (**H**) and Kaplan–Meier survival curves (**I**) of C57BL/6 mice inoculated with 1×10^5 VC or Setdb1KO B16F10 cells. Radiotherapy (1×8 Gy) was conducted 7 days after inoculation of the tumor cells. Error bars, SEM in **B, C, E,** and **H**. *, $P < 0.05$; **, $P < 0.01$; ***, $P < 0.001$; ns, not significant; *P* values were determined by an unpaired *t* test and log-rank test in **B** and **C**, two-way ANOVA in **E** and **H**, and log-rank test in **F** and **I**, respectively.

Taken together, we concluded that SETDB1 deficiency promoted general innate immune signaling and intratumoral lymphocyte infiltration in both human and murine tumors.

SETDB1 deficiency caused enhanced basal- and radiation-induced ERV activation and type I interferon response

We next sought to understand how SETDB1 deficiency promoted immune signaling and increased intratumoral lymphocyte infiltration. Previous studies report that SETDB1, as a histone H3K9 methyltransferase, plays a critical role in silencing ERVs transcription by maintaining H3K9 trimethylation and heterochromatin status (29–31). Therefore, we reasoned that SETDB1 deficiency might cause H3K9 demethylation and activation of the ERVs. To test our hypothesis, we next measured basal and radiation-induced dsRNA levels in the cytoplasm of A549 and A375 cancer cells and murine B16F10 cells by use of the well-established J2 antibody, which binds specifically to dsRNA that are 40 bp or longer (32). We observed significant increases in dsRNA levels in A549 cells on days 3, 5, and 7 after radiation exposure, peaking on day 5 (Supplementary Fig. S3A and S3B). We next used qRT-PCR to quantify known individual ERVs in irradiated A549 cells to obtain definitive evidence of radiation-induced ERV expression. Our data indicated that all 12 ERVs examined were

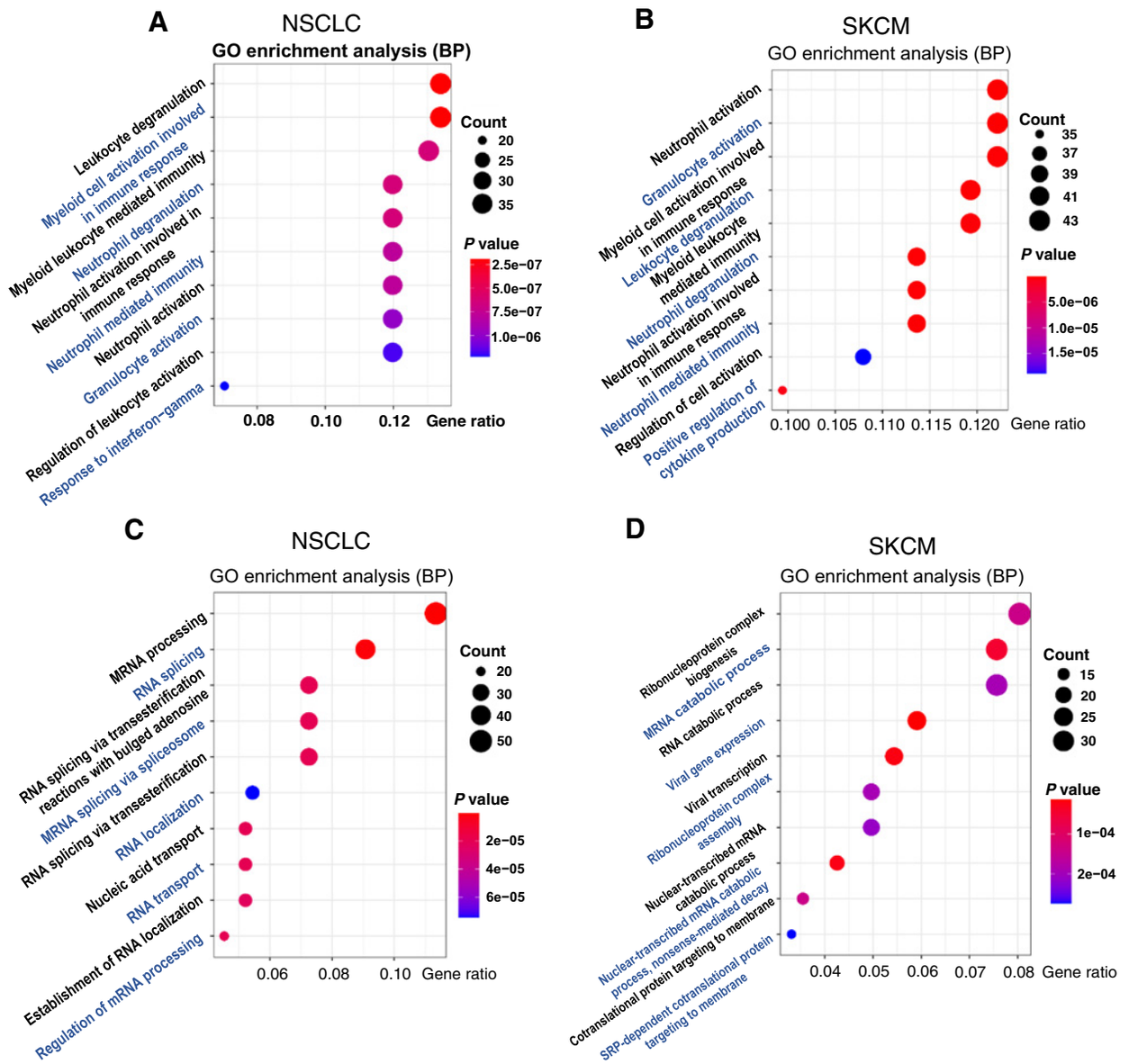

Figure 3.

GO analysis of top pathways overrepresented in SETDB1 expression-low and -high patients from RNA-seq of pretreatment tumor tissues. **A** and **B,** Top 10 GO biological processes overrepresented in SETDB1 expression-low TCGA NSCLC (**A**) and SKCM (**B**) patients. **C** and **D,** Top 10 GO biological processes overrepresented in SETDB1 expression-high TCGA NSCLC (**C**) and SKCM (**D**) patients. *P* values were determined by an unpaired *t* test.

induced by radiation exposure, and the induction peaked at day 5 (Supplementary Fig. S3C–S3N).

We next determined radiation-induced dsRNA in SETDB1-deficient A549 lung cancer and A375 melanoma cells at day 5 post-irradiation. Our data indicate that both basal and radiation-induced cytoplasmic dsRNA levels were significantly increased in SETDB1-knockout A549 (**Fig. 5A** and **B**; Supplementary Fig. S4), and A375 cells (**Fig. 5C** and **D**). We also found that in B16F10 cells, Setdb1 knockout enhanced both basal or radiation-induced dsRNA (Supplementary Fig. S5A and S5B).

We next analyzed the correlation between SETDB1 and individual ERV expression levels in NSCLC and SKCM patients in the TCGA database. Our analysis indicated that expression levels of some ERVs were significantly higher in SETDB1 low-expressing NSCLC (**Fig. 6A–D**) and SKCM tumors (**Fig. 6E** and **F**).

We further used qRT-PCR was used to quantify individual ERV induction in SETDB1-deficient A549 and A375 cells. Our data showed significantly higher levels of both basal and radiation-induced ERV transcription for most ERVs examined in SETDB1-deficient A549 (**Fig. 6G–J**; Supplementary Fig. S4) and A375 (**Fig. 6K–N**) cells. Previous studies have indicated ERV activation can induce a viral mimicry state and trigger type I interferon response (13, 14). We thus quantified the transcription levels of several interferon-stimulated genes (ISG) in control and irradiated A549 and A375 cells. Consistent

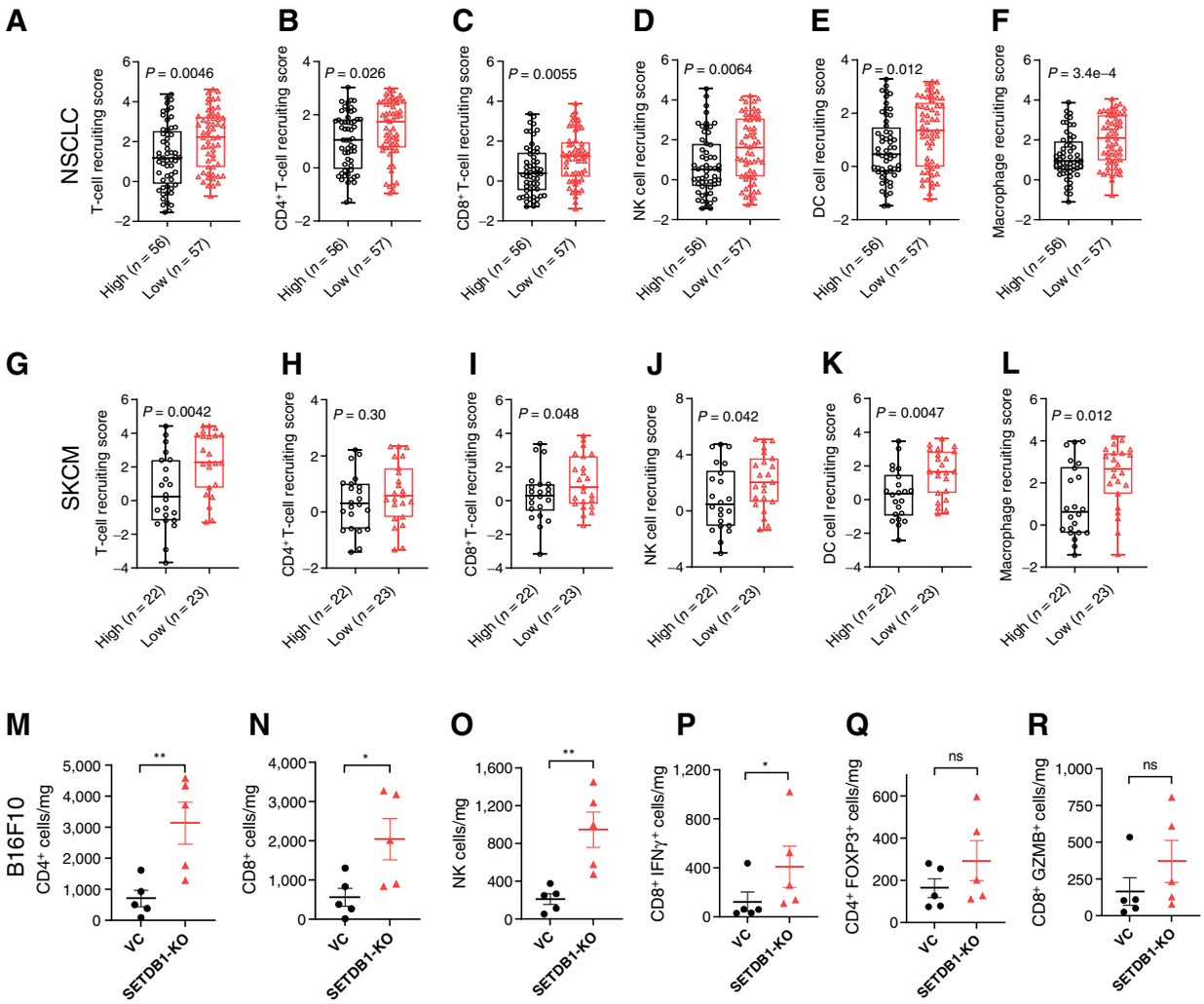

Figure 4.

The influence of SETDB1 expression on lymphocyte activation and infiltration in human and mouse tumors. **A–L,** Tumor lymphocyte recruitment scores in SETDB1-high vs. -low NSCLC (**A–F**) and SKCM (**G–L**) patients. Data obtained from CIBERSORT analysis of RNA-seq data of pretreatment tumor tissues. Cutoff values between high and low groups are medians. The box plots show median ± IQR (interquartile range). **M–R,** The average numbers of tumor-infiltrating $CD4^+$ T cells (**M**), $CD8^+$ T cells (**N**), NK cells (**O**), $CD4^+FOXP3^+$ Tregs (**P**), $CD8^+IFN\gamma^+$ T cells (**Q**), and $CD8^+GZMB^+$ T cells (**R**) per mg of tissue from vector control (VC) or SETDB1-KO B16F10 tumors grown in C57BL/6 mice. Flow cytometry analyses were done on day 14 after implantation of 1×10^5 tumor cells. In **M–R**, values indicate mean ± SEM. *, $P < 0.05$; **, $P < 0.01$; ns, not significant; P values were determined by an unpaired t test.

with ERV induction, radiation induced significant increases in ISG expression, and SETDB1 deficiency enhanced basal ERV levels significantly in A549 (**Fig. 6O–S**) and A375 (**Fig. 6T–X**) cells. In addition, radiation further boosted already high basal ERV levels in the SETDB1KO cells. Consistently, in control and Setdb1-deficient murine B16F10 melanoma cells, radiation exposure enhanced both ERV (Supplementary Fig. S5C) and ISG (Supplementary Fig. S5D–S5H) induction.

To establish a causal relationship between SETDB1 and radiation-induced viral mimicry and type I interferon response, we treated control and SETDB1KO A549 cells with a combination of anti-retroviral drugs, tenofovir and emtricitabine, which have previously been shown to inhibit ERV activation in human cancer cells (16). Our results show that this combination anti-retroviral pretreatment could restrain SETDB1-deficiency–enhanced, radiation-induced ERVs (Supplementary Fig. S6A–S6D) and ISGs (Supplementary Fig. S6E–S6I) in A549 cells.

We next examined the influence of radiation exposure on SETDB1 levels. Western blot analysis of irradiated A549 cells indicated that radiation caused a progressive decrease in SETDB1 levels in A549 cells, which was accompanied by attenuated $H3K9Me^3$ levels (Supplementary Fig. S7A), indicative of the derepression of the heterochromatin that was consistent with earlier reports of radiation-induced chromatin relaxation (33, 34). In addition, our data also showed that SETDB1 knockout increased radiation-induced MDA5 and IRF7 levels, two crucial factors in viral mimicry-induced type I interferon response in A549 cells (Supplementary Fig. S7B). What is the potential mechanism of radiation-induced SETDB1 attenuation? Previously, it was discovered that genotoxic stress such as radiation could induce the degradation of phosphorylated KAP1 (35). Since it is well established that

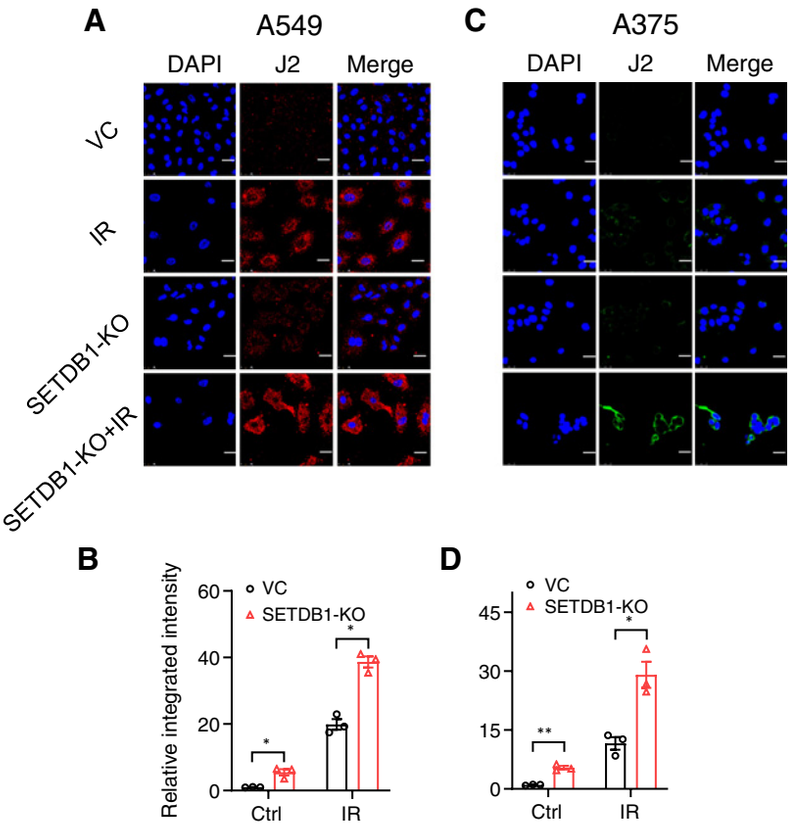

Figure 5.
Visualization and quantification of radiation-induced dsRNA levels in control and SETDB1-KO cancer cells. Representative immunofluorescence images and relative integrated immunofluorescence intensities of dsRNA-specific J2 antibody staining in control and SETDB1-KO A549 (**A** and **B**), and A375 (**C** and **D**) at 5 days after exposure to 8-Gy X-rays. Scale bar, 25 μm. *, $P < 0.05$; **, $P < 0.01$.

SETDB1 associates with KAP1 to maintain the heterochromatin (36), it is reasonable to suggest that under genotoxic stress, SETDB1 might also be degraded by the proteasome system. Indeed, when we used MG132, a well-established proteasome inhibitor together with radiation, the reduction in SETDB1 was almost abrogated, accompanied by the restoration in $H3K9me^3$ levels (Supplementary Fig. S7C). Our results, therefore, suggest that SETDB1 levels are regulated by the proteasome system after radiation exposure. In this respect, there remain critical unanswered questions, such as the role of KAP1 in regulating SETDB1 levels and the specific E3 ligases involved in mediating SETDB1 degradation. In future studies, it would be important to better understand radiation-induced heterochromatin relaxation and ERV upregulation.

Taken together, our experiments here provided strong evidence for radiation-induced ERV activation in cancer cells strongly amplified by SETDB1 inhibition.

ERV activation–induced viral mimicry essential for SetDB1 deficiency–induced radiosensitization *in vivo*

Now that we have shown evidence that SETDB1 deficiency amplified both basal and radiation-induced viral mimicry and type I interferon response, the next two important questions are: (i) To what extent ERV activation is responsible for radiation-induced type I interferon response? (ii) Are radiation-induced viral mimicry and type I interferon response functionally required for SetDB1 deficiency–induced radiosensitization to tumors? We generated SETDB1/MDA5, SETDB1/MAVS, and SETDB1/IRF7 double knockout A549 cells (**Fig. 7A**) because MDA5, MAVS, and IRF7 are well-known factors essential for ERV sensing and signaling. Control, SETDB1 single knockout, SETDB1/MDA5 or /MAVS, /IRF7 double knockout A549 cells were then subjected to X-ray exposure and analyzed (by qRT-PCR) for type I interferon response. Our data indicated that in the absence of dsRNA-sensing MDA5/MAVS/IRF7, SETDB1 deficiency induction of both the type I interferon (IFNB1) and other ISGs (IFI27, IFI44, and IFI44L) attenuated significantly (**Fig. 7B–E**).

The importance of viral mimicry and dsRNA-sensing type I interferons was further supported by *in vitro* proliferation and radiation sensitivity assays. Using EdUrd labeling and staining with dsRNA-specific J2 antibody, we observed a significantly higher fraction of J2 staining in EdU-negative cells (Supplementary Fig. S8A and S8B). Because EdUrd only stains proliferating cells, these results thus indicate that radiation-induced ERV activation correlated with proliferation arrest in irradiated A549 cells. Colony formatting assays further bolstered these results in A549 cells. These assays showed that the radiosensitivity observed in SETDB1-KO A549 cells was significantly attenuated by the double knockout of MDA5, MAVS, or IRF7 genes (Supplementary Fig. S8C).

To determine the functional importance of dsRNA-induced type I interferons in the radiation response of Setdb1-deficient tumors *in vivo*, we conducted radiotherapy experiments with tumors established from B16F10 cells deficient in Setdb1. We used an anti-interferon receptor (IFNAR) antibody to block type I interferon response. Our results showed that using the anti-IFNAR antibody reduced tumor growth delay in nonirradiated Setdb1-deficient tumors significantly (**Fig. 7F**). Furthermore, it also abrogated radiation-induced growth delay of Setdb1-deficient tumors (**Fig. 7F–G**). To assess the importance of the immune effector cells in SetDB1 deficiency–induced radiosensitization, we depleted $CD4^+$T, $CD8^+$T, and NK cells using anti-CD4, anti-CD8, and anti-NK1.1 antibodies,

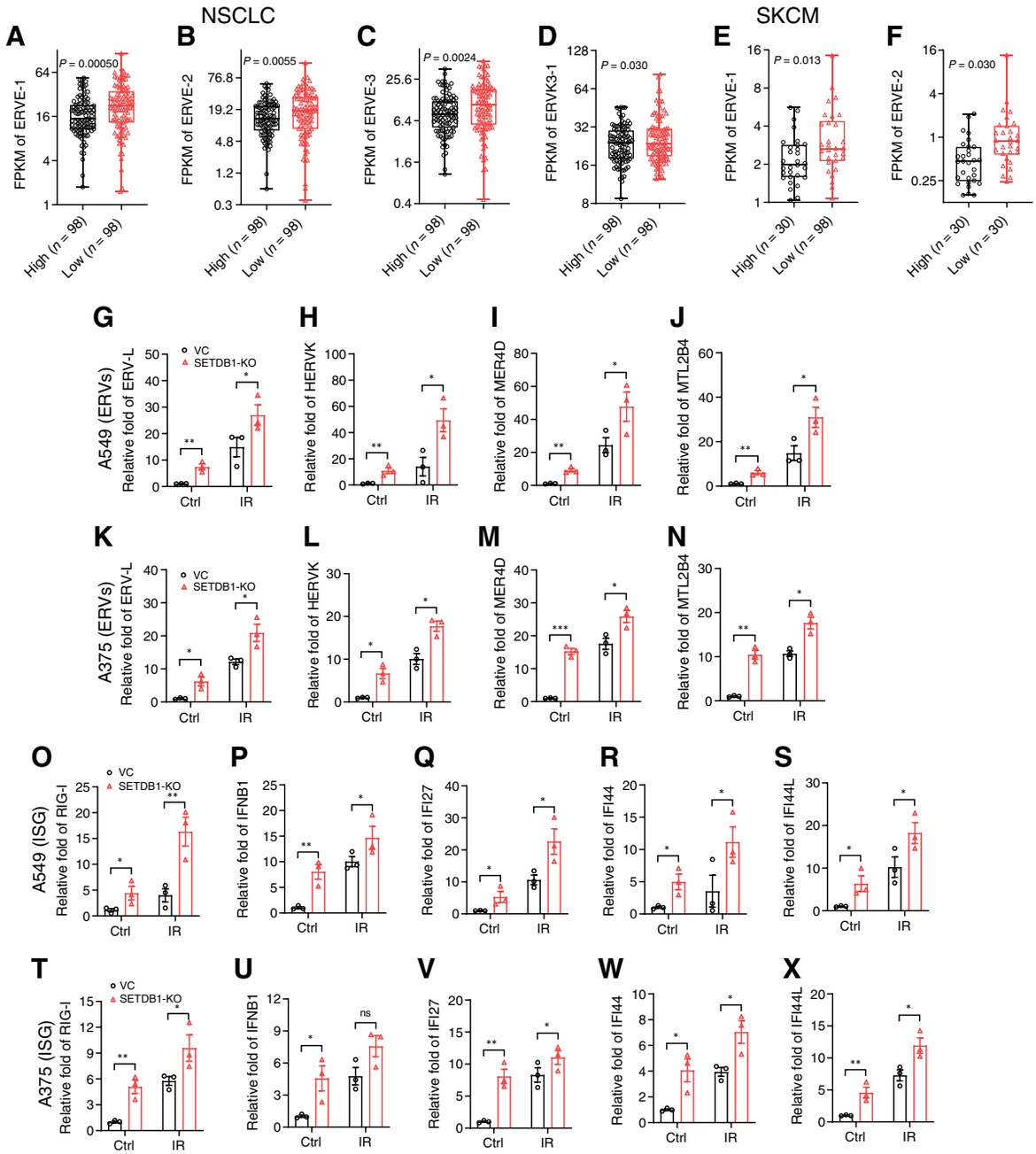

Figure 6.

SETDB1 deficiency enhanced basal and radiation-induced ERV activation and type I interferon expression. **A–F,** FPKM of ERV expression levels in SETDB1-high vs. -low TCGA NSCLC (**A–D**) and SKCM (**E** and **F**) patients. Cutoff values are the top vs. lowest 20%. The box plots show median ± IQR (interquartile range). *P* values were calculated by log-rank test. **G–N,** Relative ERV expression levels in A549 (**G–J**) and A375 (**K–N**) cells as measured by qRT-PCR in VC and SETDB1-KO cells at 5 days after exposure to 8 Gy of X-rays. **O–X,** Relative type I interferon response genes' expression levels in A549 (**O–S**) and A375 (**T–X**) as measured by qRT-PCR in VC and SETDB1-KO cells at 5 days after exposure to 8 Gy of X-rays. Quantitative values in **G–X** are shown as mean ± SEM. *, $P < 0.05$; **, $P < 0.01$; ***, $P < 0.001$; ns, not significant, as determined by an unpaired *t* test.

respectively, in another series of tumor growth delay experiments. Our results indicated that depletion of any one of the three cellular subsets abrogated SetDB1 deficiency indued radiosensitization of B16F10 tumors (**Fig. 7H–I**). Consistently, in athymic nude mice, which are deficient in T cells, SETDB1 deficiency-induced tumor growth delay and radiotherapy benefits were significantly attenuated compared with wild-type C57BL/6 mice (Supplementary Fig. S8D–S8E vs. **Fig. 2H–I**). Finally, MAVS deficiency by itself had a modest but significant effect in attenuating radiation-induced tumor suppression in wild-type B16F10 models (Supplementary Fig. S8F–S8H).

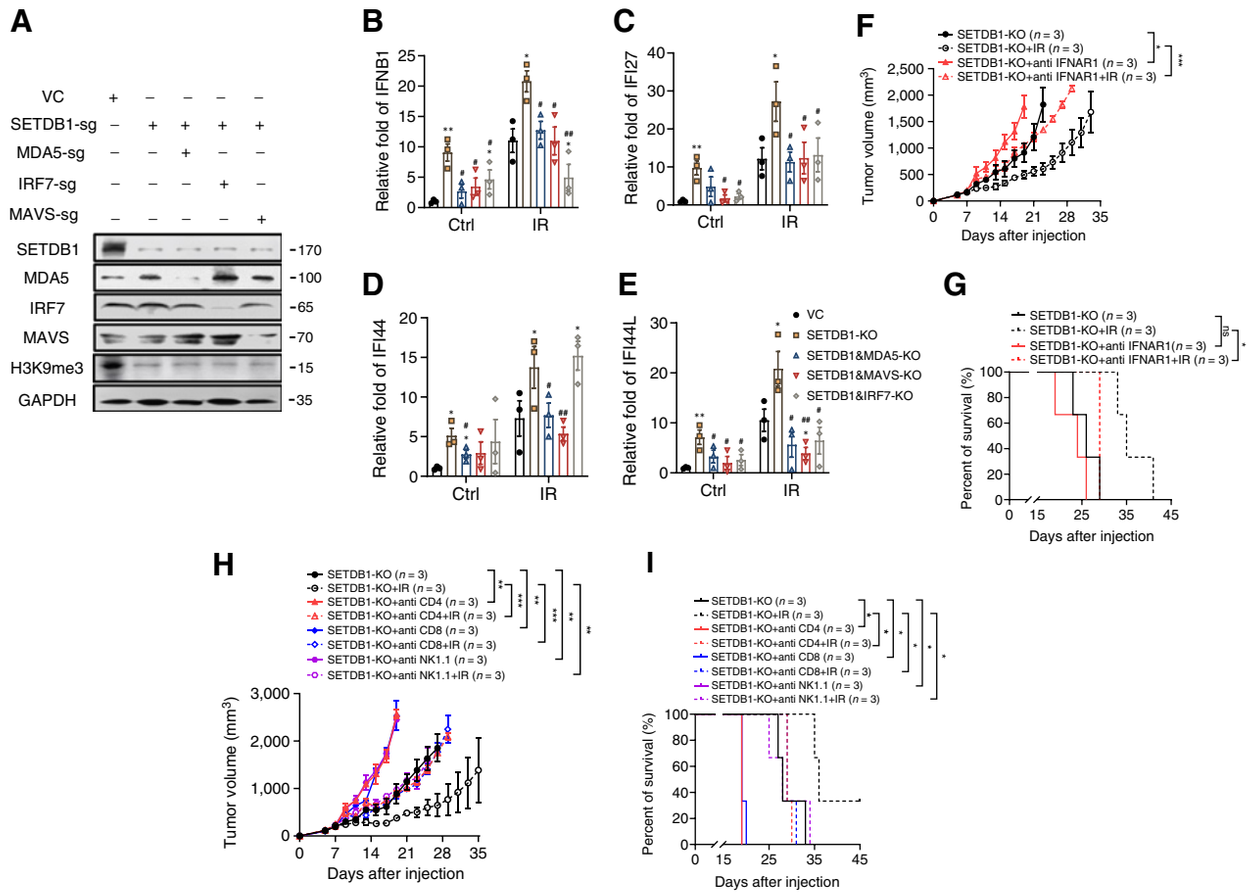

Figure 7.

ERV-induced type I interferon response responsible for increased radiotherapy-induced tumor growth in SETDB1-deficient tumors. **A,** Western blot analyses for MDA5, MAVS, IRF7, and H3K9me^3 levels in VC and SETDB1-KO A549 cells with or without double knockdown of MDA5, IRF7, or MAVS. **B–E,** Relative expression levels of type interferon response genes in SETDB1-KO, SETDB1/MDA5-DKO, SETDB1/MAVS-DKO, and SETDB1/IRF7-DKO A549 cells at 5 days after exposure to 0 and 8-Gy X-rays, as measured by qRT-PCR. **F** and **G,** Tumor growth delay (**F**) and Kaplan–Meier survival curve (**G**) of C57BL/6 mice inoculated with 1×10^5 control or SETDB1-KO B16F10 cells treated with or without anti-IFNAR antibodies (200 μg/mouse) on days 6, 9, 12, and irradiated with or without 8-Gy X-rays on day 7 after inoculation. **H** and **I,** Tumor growth delay (**H**) and Kaplan–Meier survival curve (**I**) of C57BL/6 mice inoculated with 1×10^5 SetDB1-KO B16F10 cells treated with or without anti-CD4, CD8, NK1.1 antibodies, respectively (100 μg/mouse on days 1, 4, 7) and irradiated with or without 8 Gy of X-rays on day 7. Values in **B–E**, **F**, and **H** indicate mean ± SEM. *, $P < 0.05$; **, $P < 0.01$; ***, $P < 0.001$; #, $P < 0.05$, ##, $P < 0.05$ (compared with the SETDB1 KO group); ns, not significant, as determined by two-way ANOVA in **F** and **H**. In **B–E**, *P* values were determined by an unpaired *t* test. In **G** and **I**, *P* values were determined by the log-rank test.

Together, our results showed the importance of the dsRNA-sensing signaling pathway in mediating SETDB1 deficiency-induced radiosensitization (*in vitro* and *in vivo*) and the importance of an intact immune system *in vivo*.

Discussion

Identifying innate cellular immunity signaling, such as the cytoplasmic dsDNA-sensing cGAS/STING pathway, as a critical signaling event in determining tumor response to radiotherapy is a landmark discovery. It provides a critical mechanistic understanding of how radiation-induced DNA damage can influence tumor response to radiotherapy and highlights a direct link between DNA DSBs and the host immune system. From this perspective, radiation-induced ERV activation added an important new twist to the interaction between radiation and the cellular innate immune system. Together with our recent identification of KAP1 as an important regulator of ERV activation during radiotherapy (37), the present study provides solid proof for a potential role of the KAP1/SETDB1 complex in suppressing ERV when mammalian cells suffer DNA DSB damage. Compared with KAP1, an adaptor protein responsible for bringing other proteins together to promote H3K9 trimethylation (36) and difficult to target, SETDB1 is an effector histone trimethyltransferase with clearly defined enzymatic activities. Because histone methyltransferase inhibitors have been successfully developed and are currently in human clinical trials (38), SETDB1 should be much more amenable to drug development than KAP1.

The discovery of the radio-sensitizing effect of SETDB1 inhibition is exciting from several different perspectives. First, it provides a novel druggable therapeutic target for radiotherapy different from well-established radio-sensitizing targets such as DNA double-strand repair factors ATM and DNA-PKcs (39). Second, targeting SETDB1

mobilizes the immune system to fight cancer by activating the dsRNA-sensing innate immune signaling pathway, which is quite novel among other radio-sensitizing targets currently in consideration. Given the recent advances in our understanding of the importance of the immune system in radiotherapy (2), our discovery provides another exciting angle to understand and exploit cancer radiotherapy. Third, since ERVs and other retroviral elements exist in all human cells, SETDB1-targeting may be applicable to all cancer types where radiotherapy is used.

Moving forward, we still have some important unanswered issues concerning the prospect of SETDB1 as a target for the radiosensitization of tumors. One key question is whether normal cells respond similarly to tumor cells in ERV activation. Although both normal and malignant cells repair DNA DSBs using the same DNA repair machinery, there are reasons to believe that important differences between the two may affect how ERVs are regulated. For example, after radiation exposure, p53 is induced by DNA damage to stop the cell cycle in normal cells (40). In addition, p53 can suppress the transcription of ERVs (41) and other transposable elements (42) in normal mammalian cells. On the other hand, most tumor cells are defective in p53 signaling, rendering them more susceptible to radiation-induced ERV induction. Therefore, p53 status may be an important consideration in potential future SETDB1-targeted therapeutics development.

There are limitations to our present study. One example is the radiation dosage we used. We have chosen a single dosage of 8 Gy because it elicited a robust ERV and type I interferon response in both human and mouse cells we used. Although we are confident of the capacity of clinically relevant, fractionated radiation (e.g., 1.5–2.0 Gy per day for multiple days) to induce ERVs, further systematic studies are needed to characterize the time course and kinetics of fractionated radiotherapy-mediated ERV induction. Another unanswered question of our study is the potential involvement of other transposable retroelements in the genome, such as long/short interspersed elements (SINES/LINES), which are also regulated by SETDB1 (29, 43), in causing viral mimicry and type I interferon response. It is possible that these elements, in addition to ERVs, are also involved. Future studies are warranted to tease out the relative involvement of various classes of retroelements in radiation-induced antitumor immunity.

Conclusion

Our study provides strong evidence that SETDB1 restrains radiation-induced viral mimicry state in mammalian cells and ensuing MDA5/MAVS/IRF7 mediated type I interferon response. Therefore, targeting SETDB1 may, thus, be a promising strategy to enhance the efficacy of radiotherapy by activating antitumor immunity.

Authors' Disclosures

C. Li reports grants from NIH during the conduct of the study. No disclosures were reported by the other authors.

Authors' Contributions

D. Pan: Conceptualization, formal analysis, validation, methodology, writing–original draft, writing–review and editing. **X. Bao:** Resources, data curation, investigation, methodology. **M. Hu:** Investigation, methodology. **M. Jiao:** Investigation, methodology. **F. Li:** Supervision, investigation, methodology. **C.-Y. Li:** Conceptualization, resources, supervision, funding acquisition, writing–original draft, writing–review and editing.

Acknowledgments

The authors thank Michael Cook and colleagues at the Flow Cytometry Shared Resource of Duke Cancer Institute and Yasheng Gao and colleagues at the Microscopy Shares Resource of Duke University School of Medicine for their expert services. The study is supported in part by NIH grants CA208852, CA216876, CA251439 (to C.-Y. Li), and P30CA014236 (to M.B. Kastan).

The publication costs of this article were defrayed in part by the payment of publication fees. Therefore, and solely to indicate this fact, this article is hereby marked "advertisement" in accordance with 18 USC section 1734.

Note

Supplementary data for this article are available at Cancer Research Online (http://cancerres.aacrjournals.org/).

Received October 17, 2021; revised March 13, 2022; accepted May 23, 2022; published first May 31, 2022.

References

1. Demaria S, Golden EB, Formenti SC. Role of local radiation therapy in cancer immunotherapy. JAMA Oncol 2015;1:1325–32.
2. Formenti SC, Demaria S. Combining radiotherapy and cancer immunotherapy: a paradigm shift. J Natl Cancer Inst 2013;105:256–65.
3. Twyman-Saint Victor C, Rech AJ, Maity A, Rengan R, Pauken KE, Stelekati E, et al. Radiation and dual checkpoint blockade activate non-redundant immune mechanisms in cancer. Nature 2015;520:373–7.
4. Patel SA, Minn AJ. Combination cancer therapy with immune checkpoint blockade: mechanisms and strategies. Immunity 2018;48:417–33.
5. Li XD, Wu J, Gao D, Wang H, Sun L, Chen ZJ. Pivotal roles of cGAS-cGAMP signaling in antiviral defense and immune adjuvant effects. Science 2013;341:1390–4.
6. Deng L, Liang H, Burnette B, Beckett M, Darga T, Weichselbaum RR, et al. Irradiation and anti-PD-L1 treatment synergistically promote antitumor immunity in mice. J Clin Invest 2014;124:687–95.
7. Deng L, Liang H, Xu M, Yang X, Burnette B, Arina A, et al. STING-dependent cytosolic DNA sensing promotes radiation-induced type I interferon-dependent antitumor immunity in immunogenic tumors. Immunity 2014;41:843–52.
8. Burnette BC, Liang H, Lee Y, Chlewicki L, Khodarev NN, Weichselbaum RR, et al. The efficacy of radiotherapy relies upon induction of type i interferon-dependent innate and adaptive immunity. Cancer Res 2011;71:2488–96.
9. Harding SM, Benci JL, Irianto J, Discher DE, Minn AJ, Greenberg RA. Mitotic progression following DNA damage enables pattern recognition within micronuclei. Nature 2017;548:466–70.
10. Vanpouille-Box C, Alard A, Aryankalayil MJ, Sarfraz Y, Diamond JM, Schneider RJ, et al. DNA exonuclease Trex1 regulates radiotherapy-induced tumour immunogenicity. Nat Commun 2017;8:15618.
11. Bannert N, Kurth R. The evolutionary dynamics of human endogenous retroviral families. Annu Rev Genomics Hum Genet 2006;7:149–73.
12. Grandi N, Tramontano E. Human endogenous retroviruses are ancient acquired elements still shaping innate immune responses. Front Immunol 2018;9:2039.
13. Chiappinelli KB, Strissel PL, Desrichard A, Li H, Henke C, Akman B, et al. Inhibiting DNA methylation causes an interferon response in cancer via dsRNA including endogenous retroviruses. Cell 2015;162:974–86.
14. Roulois D, Loo Yau H, Singhania R, Wang Y, Danesh A, Shen SY, et al. DNA-demethylating agents target colorectal cancer cells by inducing viral mimicry by endogenous transcripts. Cell 2015;162:961–73.
15. Griffin GK, Wu J, Iracheta-Vellve A, Patti JC, Hsu J, Davis T, et al. Epigenetic silencing by SETDB1 suppresses tumour intrinsic immunogenicity. Nature 2021;595:309–14.
16. Lima-Junior DS, Krishnamurthy SR, Bouladoux N, Collins N, Han SJ, Chen EY, et al. Endogenous retroviruses promote homeostatic and inflammatory responses to the microbiota. Cell 2021;184:3794–811.

17. Cerami E, Gao J, Dogrusoz U, Gross BE, Sumer SO, Aksoy BA, et al. The cBio cancer genomics portal: an open platform for exploring multidimensional cancer genomics data. Cancer Discov 2012;2:401–4.
18. Hoadley KA, Yau C, Hinoue T, Wolf DM, Lazar AJ, Drill E, et al. Cell-of-origin patterns dominate the molecular classification of 10,000 tumors from 33 types of cancer. Cell 2018;173:291–304.
19. Rooney MS, Shukla SA, Wu CJ, Getz G, Hacohen N. Molecular and genetic properties of tumors associated with local immune cytolytic activity. Cell 2015; 160:48–61.
20. Yu G, Wang LG, Han Y, He QY. clusterProfiler: an R package for comparing biological themes among gene clusters. OMICS 2012;16:284–7.
21. Cong L, Zhang F. Genome engineering using CRISPR-Cas9 system. Methods Mol Biol 2015;1239:197–217.
22. Puchtler H, Waldrop FS, Conner HM, Terry MS. Carnoy fixation: practical and theoretical considerations. Histochemie 1968;16:361–71.
23. Lambrechts D, Wauters E, Boeckx B, Aibar S, Nittner D, Burton O, et al. Phenotype molding of stromal cells in the lung tumor microenvironment. Nat Med 2018;24:1277–89.
24. Cong L, Ran FA, Cox D, Lin S, Barretto R, Habib N, et al. Multiplex genome engineering using CRISPR/Cas systems. Science 2013;339:819–23.
25. Ashburner M, Ball CA, Blake JA, Botstein D, Butler H, Cherry JM, et al. Gene ontology: tool for the unification of biology. the gene ontology consortium. Nat Genet 2000;25:25–9.
26. Gene Ontology C. The Gene Ontology resource: enriching a GOld mine. Nucleic Acids Res 2021;49:D325–D34.
27. Newman AM, Liu CL, Green MR, Gentles AJ, Feng W, Xu Y, et al. Robust enumeration of cell subsets from tissue expression profiles. Nat Methods 2015; 12:453–7.
28. Xu L, Deng C, Pang B, Zhang X, Liu W, Liao G, et al. TIP: a web server for resolving tumor immunophenotype profiling. Cancer Res 2018;78: 6575–80.
29. Matsui T, Leung D, Miyashita H, Maksakova IA, Miyachi H, Kimura H, et al. Proviral silencing in embryonic stem cells requires the histone methyltransferase ESET. Nature 2010;464:927–31.
30. Karimi MM, Goyal P, Maksakova IA, Bilenky M, Leung D, Tang JX, et al. DNA methylation and SETDB1/H3K9me3 regulate predominantly distinct sets of genes, retroelements, and chimeric transcripts in mESCs. Cell Stem Cell 2011;8: 676–87.
31. Kato M, Takemoto K, Shinkai Y. A somatic role for the histone methyltransferase Setdb1 in endogenous retrovirus silencing. Nat Commun 2018;9:1683.
32. Schonborn J, Oberstrass J, Breyel E, Tittgen J, Schumacher J, Lukacs N. Monoclonal antibodies to double-stranded RNA as probes of RNA structure in crude nucleic acid extracts. Nucleic Acids Res 1991;19:2993–3000.
33. Ziv Y, Bielopolski D, Galanty Y, Lukas C, Taya Y, Schultz DC, et al. Chromatin relaxation in response to DNA double-strand breaks is modulated by a novel ATM- and KAP-1 dependent pathway. Nat Cell Biol 2006;8:870–6.
34. Goodarzi AA, Noon AT, Deckbar D, Ziv Y, Shiloh Y, Lobrich M, et al. ATM signaling facilitates repair of DNA double-strand breaks associated with heterochromatin. Mol Cell 2008;31:167–77.
35. Kuo CY, Li X, Kong XQ, Luo C, Chang CC, Chung Y, et al. An arginine-rich motif of ring finger protein 4 (RNF4) oversees the recruitment and degradation of the phosphorylated and SUMOylated Kruppel-associated box domain-associated protein 1 (KAP1)/TRIM28 protein during genotoxic stress. J Biol Chem 2014; 289:20757–72.
36. Schultz DC, Ayyanathan K, Negorev D, Maul GG, Rauscher FJ., 3rd. SETDB1: a novel KAP-1-associated histone H3, lysine 9-specific methyltransferase that contributes to HP1-mediated silencing of euchromatic genes by KRAB zinc-finger proteins. Genes Dev 2002;16:919–32.
37. Lee AK, Pan D, Bao X, Hu M, Li F, Li CY. Endogenous retrovirus activation as a key mechanism of anti-tumor immune response in radiotherapy. Radiat Res 2020;193:305–17.
38. Rugo HS, Jacobs I, Sharma S, Scappaticci F, Paul TA, Jensen-Pergakes K, et al. The promise for histone methyltransferase inhibitors for epigenetic therapy in clinical oncology: a narrative review. Adv Ther 2020;37:3059–82.
39. Faulhaber EM, Jost T, Symank J, Scheper J, Burkel F, Fietkau R, et al. Kinase inhibitors of DNA-PK, ATM and ATR in combination with ionizing radiation can increase tumor cell death in HNSCC cells while sparing normal tissue cells. Genes (Basel) 2021;12:925.
40. Kastan MB, Onyekwere O, Sidransky D, Vogelstein B, Craig RW. Participation of p53 protein in the cellular response to DNA damage. Cancer Res 1991;51:6304–11.
41. Wang T, Zeng J, Lowe CB, Sellers RG, Salama SR, Yang M, et al. Species-specific endogenous retroviruses shape the transcriptional network of the human tumor suppressor protein p53. Proc Natl Acad Sci U S A 2007;104:18613–8.
42. Leonova KI, Brodsky L, Lipchick B, Pal M, Novototskaya L, Chenchik AA, et al. p53 cooperates with DNA methylation and a suicidal interferon response to maintain epigenetic silencing of repeats and noncoding RNAs. Proc Natl Acad Sci U S A 2013;110:E89–98.
43. Fukuda K, Shinkai Y. SETDB1-mediated silencing of retroelements. Viruses 2020;12:596.